Electronic Supplementary Information (ESI)

Compressed porous graphene particles for use as supercapacitor electrodes with excellent volumetric performance

Huan Li[a,b,‡], Ying Tao[a,b,‡], Xiaoyu Zheng[a,b,‡], Zhengjie Li[a,b], Donghai Liu[a,b], Zhao Xu[a,b], Chong Luo[c], Jiayan Luo[a,b,*], Feiyu Kang[c], Quan-Hong Yang[a,b,c,*]

[a]*Key Laboratory for Green Chemical Technology of Ministry of Education, School of Chemical Engineering and Technology, Tianjin University, Tianjin 300072, China*

[b]*Collaborative Innovation Center of Chemical Science and Engineering (Tianjin), Tianjin 300072, China*

[c]*Shenzhen Key Laboratory for Graphene-based Materials and Engineering Laboratory for Functionalized Carbon Materials, Graduate School at Shenzhen, Tsinghua University, Shenzhen 518055, China*

E-mail: qhyangcn@tju.edu.cn; jluo@tju.edu.cn.

Experimental Section

Synthesis of porous graphene particles (PGPs)

Graphite oxide colloidal suspension (2 mg mL^{-1}) was prepared by ultrasonication of graphite oxide powders (170 mg) made of modified Hummers' method in 85 mL de-ionized water, followed by centrifugation (3800 rpm for 20 min). Typically, the homogeneous GO colloid suspension was placed in a Teflon-lined autoclave, and treated by a hydrothermal process in muffle furnace (180 ^{o}C) for 6 h, resulting in a cylindrical graphene hydrogel. Such hydrogel was soaked in 20 mL KOH solution for 12 h static adsorption and subsequent vacuum drying. Then the mixture was subjected to heat treatment at 800 ^{o}C for 1 h in argon flowing condition. After cooling down to room temperature, the sample was repeatedly washed by 5 % HCl and de-ionized water, followed by drying overnight to afford the products (PGPs).

Materials characterization

The morphology of samples were captured by scanning electron microscopy (SEM) (Hitachi S4800, Japan) with accelerating voltage of 5.0 kV. Transmission electron microscopy (TEM) characterization was performed on JEM 3100F (JEOL, Japan) operated at 200 kV. X-ray diffraction (XRD) patterns were recorded on a Bruker D-8 (Cu Ka radiation, λ= 1.54056 Å) at room temperature and the data was collected from 10° to 60° with a scan rate of 10 ° min^{-1}. TGA was performed on a TG8120 by heating the samples to 800 °C at 10 °C min^{-1} in the atmosphere of nitrogen. Raman spectroscopy was recorded by a multi-

wavelength micro-Raman spectroscope (JY HR800) using 532.05 nm incident radiation and a 50× aperture. N_2 adsorption-desorption isotherms (77 K) were measured by Belsorp-Mini instrument (BEL, Inc, Japan). Samples of approximately 50 mg were heated at 200 ºC under vacuum to remove all the adsorbed species. Specific surface area and pore size distribution were performed by Brunauer-Emmett-Teller (BET) and Density Function Theories (DFT) method, respectively.

Electrochemical measurements

Symmetrical two-electrode cell configuration was used to measure the performance of PGPs as supercapacitor electrode. PGPs were mixed with polytetrafluoroethylene (binder) with a mass ratio of 97:3 without conductive additives. The mixture was ground up with mortar and pestle, rolled into 120 μm thick raw films and punched into 1 cm diameter electrode. Then raw films were compressed by 10 MPa (91 μm thick), 25 MPa (67 μm thick) and 40 MPa (55 μm thick). And the corresponding electrode density was 0.55 g cm^{-3} (PGPs-10 MPa), 0.75 g cm^{-3} (PGPs-25 MPa) and 0.92 g cm^{-3} (PGPs-40 MPa) while density of uncompressed electrode was 0.42 g cm^{-3} (PGPs-0 MPa). Two nearly identical electrodes were assembled in a test cell consisting of two electrodes, two current collectors and an ion separator supported by two stainless steel plates. The assembly of test cell in ionic liquid ($BMIMBF_4$) was carried out in a glove box filled with Ar. Electrochemical impedance spectroscopy, cyclic voltammetry and galvanostaric charge-discharge test were performed on electrochemical workstation (Metrohm, Switzerland) and LAND (Wuhan, China).

The specific capacitance based on single electrode of the device was calculated from the galvanostatic charge-discharge curves at different current densities using the formula:

$$C_s\ (F\ g^{-1}) = 2I\Delta t/m\Delta U \quad (1)$$

Where I is the constant current applied, Δt is the discharge time, ΔU is the operating voltage and m is the net mass of the active material on single electrode.
The volumetric capacitance was calculated as:

$$C_v\ (F\ cm^{-3}) = \rho \times C_s \quad (2)$$

Where ρ is the electrode density and C_s is the specific capacitance of the single electrode.
The volumetric energy density of two electrodes was calculated as:

$$E_{vol}\ (Wh\ L^{-1}) = 0.125C_v\Delta U^2/3.6 \quad (3)$$

Where C_v is the volumetric capacitance of electrode and ΔU is the operating voltage.
The volumetric power density was calculated as:

$$P_{vol}\ (W\ L^{-1}) = E_{vol}/\Delta t \quad (4)$$

Where E_{vol} is the volumetric energy density and Δt is the discharge time.

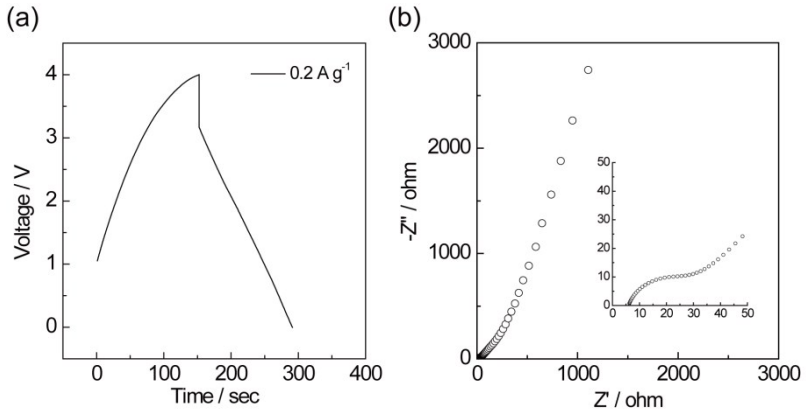

Fig. S1 Electrochemical performance of HPGM in $BMIMBF_4$ electrolyte. (a) Charge-discharge curves at 0.2 A g^{-1}. (b) Nyquist plot and the inset shows the high-frequency region. HPGM electrode only shows a C_v of 22 F cm^{-3} at 0.2 A g^{-1} and Nyquist plot in low-frequency region shows a limited capacitive properties.

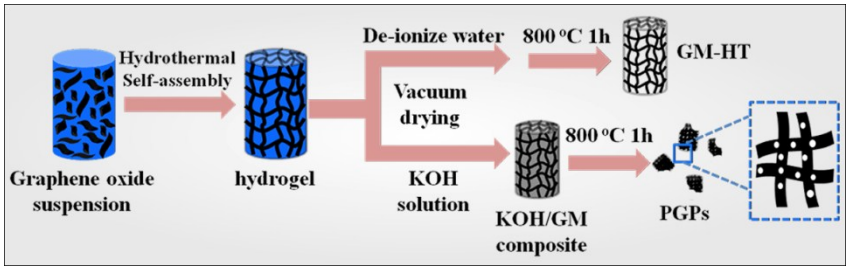

Fig. S2 Scheme of preparation routes for preparing of PGPs

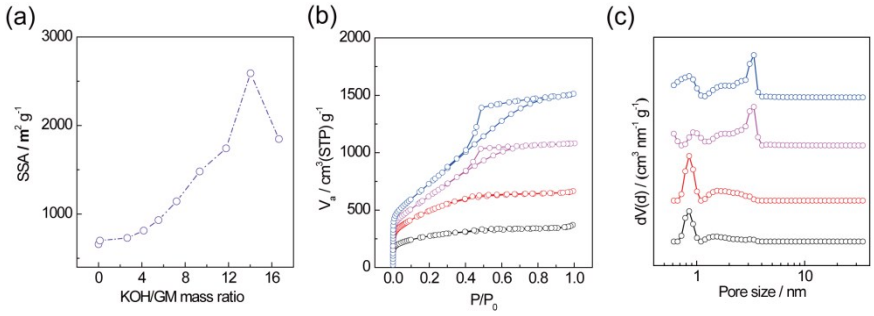

Fig. S3 (a) BET specific surface area (SSA) of PGPs varied from KOH/GM mass ratio and (b) N_2 adsorption-desorption isotherms (77 K) and (c) pore size distribution calculated by DFT model of typical activated samples. The activated products can reach 945 $m^2 g^{-1}$, 1742 $m^2 g^{-1}$, 2590 $m^2 g^{-1}$ and 2126 $m^2 g^{-1}$ corresponding to the KOH/GM mass ratio of 5.5, 11.7, 14.0 and 16.6. Pore size distribution reveals that there is an obviously increase of ultramicropores less than 1 nm and mesopores around 3.5 nm.

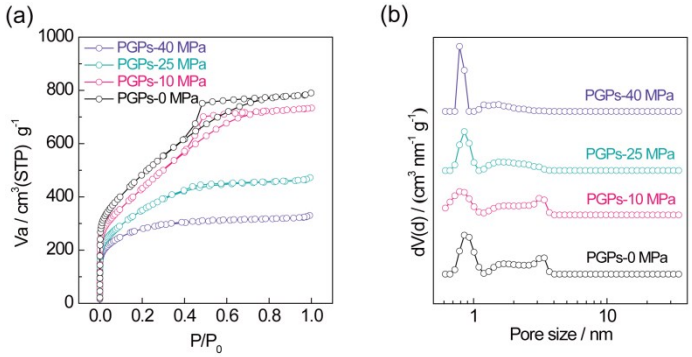

Fig. S4 N_2 adsorption-desorption isotherms (77 K) and pore size distribution of PGPs-40 MPa, PGPs-25 MPa, PGPs-10 MPa and PGPs-0 MPa electrode. The BET specific surface area of electrodes are 968 $m^2 g^{-1}$, 1232 $m^2 g^{-1}$, 1534 $m^2 g^{-1}$ 1700 $m^2 g^{-1}$ with electrode density of 0.92 g cm^{-3}, 0.75 g cm^{-3}, 0.55 g cm^{-3}, 0.42 g cm^{-3}. PGPs-40 MPa electrode shows a micropore size mainly at 0.75~0.8 nm and mesopores about 2~3 nm.

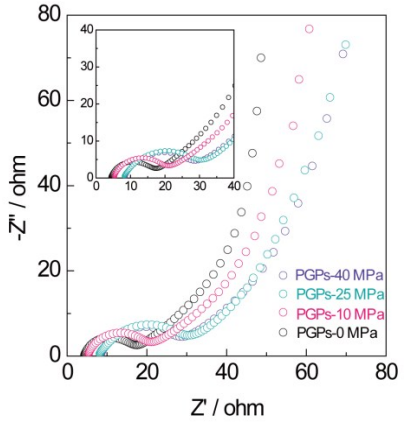

Fig. S5 Nyquist plots of PGPs based supercapacitors. Small resistance reveals excellent capacitive properties of such electrodes.

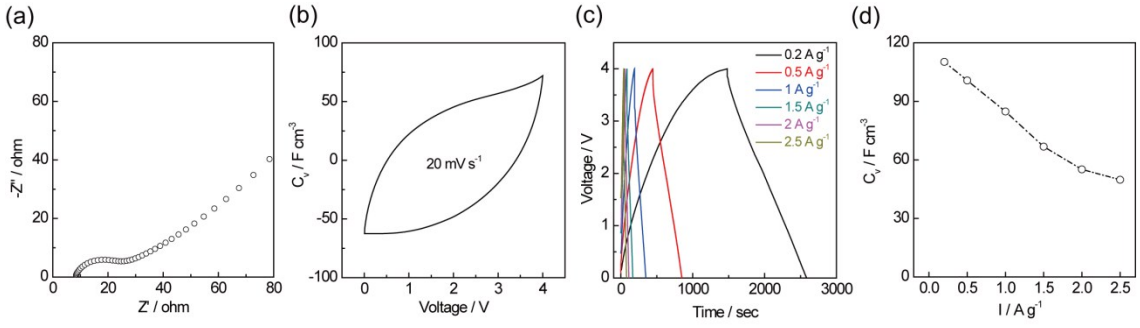

Fig. S6 Electrochemical performance of GM-HT in two-electrode $BMIMBF_4$ electrolyte system. By comparison, PGPs-40 MPa electrode shows high volumetric capacitance with superior rate performance.

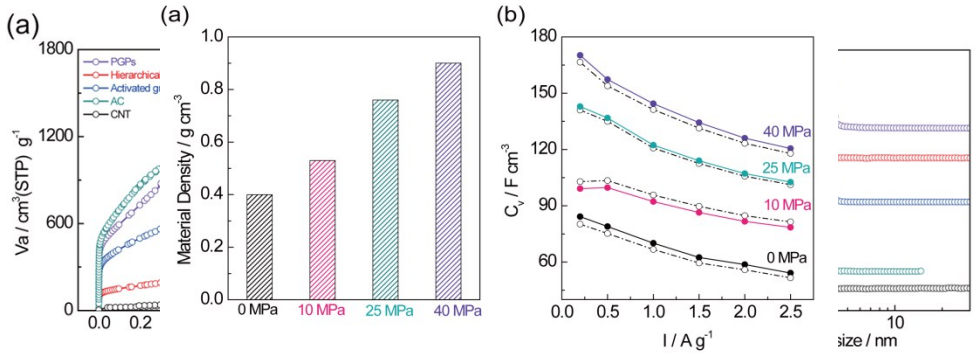

Fig. S7 (a) Compressed material density at different compression pressure; (b) Comparison of volumetric capacitance calculated based on electrode density (solid line) compressed material density (dash line).

Fig. S9 N_2 adsorption-desorption isotherms (77 K) and pore size distribution of PGPs, hierarchical porous graphene, activated graphene sheets, commercial AC and CNT. SSA of them are 2590 m^2 g^{-1}, 632 m^2 g^{-1}, 1758 m^2 g^{-1}, 3196 m^2 g^{-1}, 100 m^2 g^{-1}, respectively. PGPs show large amounts of micropores and mesopores.

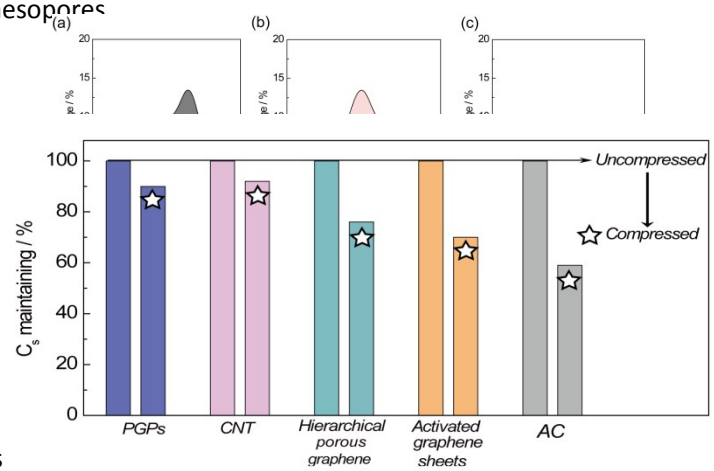

Fig. S8 (a-c) PGPs pressed electrode density and particle size; (e-f) Scheme for the compressed low-density and high-density electrode.

Fig. S10 Gravimetric capacitance-maintaining of PGPs compared to a hierarchical porous graphene, activated graphene sheets and commercial active carbon (AC).

Table S1 Compression investigations for PGPs, hierarchical porous graphene, activated graphene sheets, commercial AC and CNT electrodes. The capacitance was obtained by charge-discharge curves at 1 A g^{-1}.

	PGPs	Hierarchical graphene	Activated graphene sheet	AC	CNT
SSA / m^2 g^{-1} (Powders)	2590	632	1758	3196	100
SSA / m^2 g^{-1} (10 MPa)	1534	434	892	1843	102
Electrode density / g cm^{-3}	0.55	0.31	0.56	0.51	0.27
C_s / F g^{-1}	174	82	130	172	20
C_v / F cm^{-3}	95.7	25.42	72.8	87.72	5.4
SSA / m^2 g^{-1} (40 MPa)	968	323	615	1102	86
Electrode density / g cm^{-3}	0.92	0.56	0.84	0.89	0.34
C_s / F g^{-1}	157	62	91	101	17
C_v / F cm^{-3}	144.4	34.72	76.44	89.89	5.78

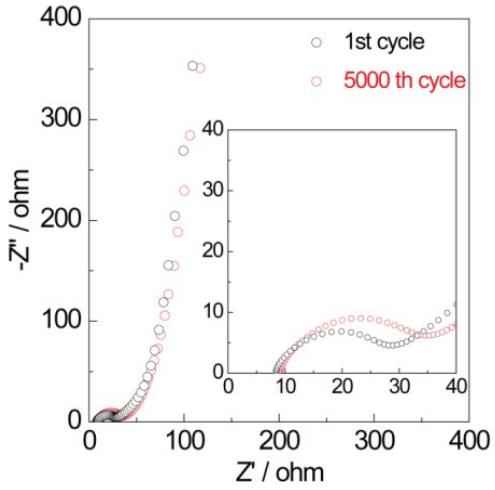

Fig. S11 Nyquist plots of PGPs-40 MPa based supercapacitor at the first cycle and the 5000th cycle after charge-discharge.

Table S2 Performance of reported electrode materials for symmetric supercapacitors

Materials reported	Material density [g cm^{-3}]	Electrolyte Operating voltage [V]	C_s [F g^{-1}]	C_v [F cm^{-3}]	P_{vol} [W L^{-1}]	E_{vol} [Wh L^{-1}]	Ref.
PGPs	0.92	BMIMBF4 4 V	185.0	170.2	184	94.6	This work
EM-CCG	1.25	$EMIMBF_4$/AN 3.5 V	167.1	208.9	~1353	~110	1
1T MoS_2	2.5	$EMIMBF_4$/MECN 3.5 V	~100	250	1100	110	2
HGF	0.71	$EMIMBF_4$/AN 3.5 V	298	212	545.4	79	3
r[GO-CNT]	1.5	$TEABF_4$/PC 3 V	109.7	165	600	51.4	4
Compressed a-MEGO	0.75	$TEABF_4$/AN 3.5 V	147	110	671.7	48	5
Ti_3C_2 Clay	3.7	H_2SO_4 1 V	245	900	247.4	37.8	6
HPGM	1.58	$TEABF_4$/AN 2.5 V	110	174	196.9	37.6	7
Curved graphene	0.3	$EMIMBF_4$ 4 V	154	46.2	300.4	25.7	8
a-MEGO	0.36	$BMIMBF_4$/AN 3.5 V	165	59.4	315.4	25.3	9
Ti_3C_2 Paper	4.9	KOH 1.1 V	~70	340	934.7	14.28	10

Notes and references

1. X. Yang, C. Cheng, Y. Wang, L. Qiu and D. Li, *Science*, 2013, **341**, 534-537.

2. M. Acerce, D. Voiry and M. Chhowalla, *Nature Nanotechnology*, 2015, **10**, 313-318.

3. Y. Xu, Z. Lin, X. Zhong, X. Huang, N. O. Weiss, Y. Huang and X. Duan, *Nature Communications*, 2014, **5**, 4554.

4. N. Jung; S. Kwon; D. Lee; D. M. Yoon; Y. M. Park; A. Benayad; J. Y. Choi; J. S. Park, *Advanced Materials* **2013,** 25, 6854-6858.

5. S. Murali, N. Quarles, L. L. Zhang, J. R. Potts, Z. Tan, Y. Lu, Y. Zhu and R. S. Ruoff, *Nano Energy*, 2013, **2**, 764-768.

6. M. Ghidiu, M. R. Lukatskaya, M. Q. Zhao, Y. Gogotsi and M. W. Barsoum, Nature, 2014, **516**, 78-81.

7. Y. Tao, X. Xie, W. Lv, D. M. Tang, D. Kong, Z. Huang, H. Nishihara, T. Ishii, B. Li, D. Golberg, F. Kang, T. Kyotani and Q. H. Yang, *Scientific Reports*, 2013, **3**, 2975.

8. C. Liu, Z. Yu, D. Neff, A. Zhamu and B. Z. Jang, *Nano letters*, 2010, **10**, 4863-4868.

9. Y. Zhu, S. Murali, M. D. Stoller, K. J. Ganesh, W. Cai, P. J. Ferreira, A. Pirkle, R. M. Wallace, K. A. Cychosz, M. Thommes, D. Su, E. A. Stach and R. S. Ruoff, *Science*, 2011, **332**, 1537-1541.

10. M. R. Lukatskaya, O. Mashtalir, C. E. Ren, Y. Dall'Agnese, P. Rozier, P. L. Taberna, M. Naguib, P. Simon, M. W. Barsoum and Y. Gogotsi, *Science*, 2013, **341**, 1502-1505.